



Published in final edited form as:

Invest Radiol. 2015 April ; 50(4): 195–204. doi:10.1097/RLI.000000000000100.

Combined DCE-MRI and DW-MRI for Predicting Breast Cancer Pathological Response After the First Cycle of Neoadjuvant Chemotherapy

Xia Li, Ph.D.¹, Richard G. Abramson, M.D.^{1,2,3}, Lori R. Arlinghaus, Ph.D.¹, Hakmook Kang, Ph.D.⁴, A. Bapsi Chakravarthy, M.D.^{3,5}, Vandana G. Abramson, M.D.^{3,6}, Jaime Farley, R.N.³, Ingrid A. Mayer, M.D.⁶, Mark C. Kelley, M.D.^{3,7}, Ingrid M. Meszoely, M.D.^{3,7}, Julie Means-Powell, M.D.^{3,6}, Ana M. Grau, M.D.^{3,7}, Melinda Sanders, M.D.^{3,8}, and Thomas E. Yankeelov, Ph.D.^{1,2,3,9,10,11}

¹ Institute of Imaging Science, Vanderbilt University, Nashville, TN, USA

²Department of Radiology and Radiological Sciences, Vanderbilt University, Nashville, TN, USA

³Vanderbilt Ingram Cancer Center, Vanderbilt University, Nashville, TN, USA

⁴Department of Biostatistics, Vanderbilt University, Nashville, TN, USA

⁵Department of Radiation Oncology, Vanderbilt University, Nashville, TN, USA

⁶Department of Medical Oncology, Vanderbilt University, Nashville, TN, USA

⁷Department of Surgical Oncology, Vanderbilt University, Nashville, TN, USA

⁸Department of Pathology, Vanderbilt University, Nashville, TN, USA

⁹Department of Physics and Astronomy, Vanderbilt University, Nashville, TN, USA

¹⁰Department of Cancer Biology, Vanderbilt University, Nashville, TN, USA

¹¹Department of Biomedical Engineering, Vanderbilt University, Nashville, TN, USA

Abstract

Objectives—To determine if combined measurements from dynamic contrast enhanced magnetic resonance imaging (DCE-MRI) and diffusion weighted MRI (DW-MRI), obtained before and after the first cycle of neoadjuvant chemotherapy (NAC), are superior to single parameter measurements for predicting pathological complete response (pCR) in breast cancer patients.

Materials and Methods—Patients with Stage II/III breast cancer were enrolled in an IRB-approved study in which 3T DCE- and DW-MRI data were acquired before ($n = 37$) and after one cycle ($n = 33$) of NAC. Estimates of K^{trans} , v_e , v_p , and k_{ep} ($= K^{trans}/v_e$) were generated from the DCE-MRI data using the Extended Tofts-Kety (ETK) model. The apparent diffusion coefficient

(ADC) was estimated from the DW-MRI data. The derived parameter k_{ep}/ADC was compared to single parameter measurements for its ability to predict pCR after the first cycle of NAC.

Results— k_{ep}/ADC after the first cycle of NAC discriminated patients who went on to achieve a pCR ($P < 0.001$), and achieved a sensitivity, specificity, positive predictive value, and area under the receiver operator curve (AUC) of 0.92, 0.75, 0.69, and 0.86, respectively. These values were superior to the single parameters k_{ep} (AUC = 0.77) and ADC (AUC = 0.81). The AUCs between k_{ep}/ADC and k_{ep} were significantly different based on the bootstrapped 95% CIs (0.0062, 0.20), while the AUCs between k_{ep}/ADC and ADC trended towards significance (−0.12, 0.24).

Conclusions—A combined analysis of DCE-MRI and DW-MRI parameters was superior to single-parameter measurements for predicting pCR after the first cycle of NAC.

Keywords

Combined DCE- and DW-MRI; breast cancer; treatment response

INTRODUCTION

Dynamic contrast enhanced magnetic resonance imaging (DCE-MRI) and diffusion weighted MRI (DW-MRI) have matured to the point where they are able to provide quantitative, and complimentary information on tumor status (1). DCE-MRI involves the serial acquisition of T_1 -weighted MR images of a tissue of interest before and after an intravenous injection of a paramagnetic contrast agent (CA). As the CA accumulates and then is eliminated, it changes the native relaxation rate of tissue water, and therefore the measured MR signal intensity. By fitting the resulting signal intensity time course to an appropriate pharmacokinetic model, physiological parameters can be extracted that relate to the volume transfer rate (K^{trans} , related to tissue perfusion and permeability), blood plasma volume fraction (v_p), extravascular extracellular volume fraction (v_e), and the efflux rate constant ($k_{ep} = K^{trans}/v_e$). DW-MRI allows for the *in vivo* measurement of the motion of water in tissue. By applying two or more diffusion-sensitizing gradients with different amplitudes, the apparent diffusion coefficient (ADC) can be estimated from the resulting DW-MRI data to describe the rate of water diffusion in cellular tissues. In well-controlled studies it has been shown that the ADC varies inversely with cell (2).

There have been many efforts employing DCE-MRI as a surrogate biomarker for assessing and predicting the response of breast tumors to neoadjuvant chemotherapy (3-9). For example, Ah-See *et al* (7) calculated the changes in pharmacokinetic parameters estimated from DCE-MRI data before and after two cycles of treatment and reported that change in K^{trans} was the best predictor of pathologic non-response, while Padhani *et al* (8) found both tumor size and change in the range of histograms in K^{trans} after two cycles of treatment were equally able to predict eventual response. There also have been studies investigating DW-MRI and some have found that the ADC is able to separate responders from non-responders after neoadjuvant chemotherapy (9-11), while some other studies showed that there is no correlation between ADC and treatment response (12,13). In some recent studies (6,14,15), both DCE- and DW-MRI data have been evaluated. However, those previous studies reported the ability of both data to monitor or assess treatment response separately and did

not show the performance of the combination of DCE- and DW-MRI. The objective of this study was to determine if a multiparametric combination of DCE- and DW-MRI data can increase accuracy for predicting pathologic complete response (pCR) in breast cancer patients undergoing neoadjuvant chemotherapy. In particular, we hypothesized that the derived measurement k_{ep}/ADC would have superior predictive accuracy than single parameter measurements in isolation. The eventual clinical goal is to be able to predict, after the first cycle of neoadjuvant chemotherapy, which patients will go on to achieve pCR.

METHODS

Patient Eligibility and Enrollment

Patients undergoing NAC for locally advanced breast cancer were eligible for this prospective, IRB-approved study. All patients had histologically documented invasive breast cancer at least 1 cm in the longest dimension with a sufficient risk of recurrence, based on pre-treatment clinical parameters of size, grade, age and nodal status, to warrant the use of NAC. Patients provided written informed consent before participating in this study.

Schema

MRI was performed prior to initiating chemotherapy (t_1), after one cycle (t_2), and after all cycles (t_3) of chemotherapy. The NAC regimen was left to the discretion of the treating oncologist based on patient factors such as menopausal status and age as well as tumor characteristics, including size, grade, nodal status and receptor status.

Pathologic Assessment of Response

pCR was defined as the absence of any invasive cancer in breast or lymph nodes. Patients with any residual invasive cancer in the breast or lymph nodes or patients who progressed prior to surgery were defined as non responders (non-pCR). Determination of pCR and non-pCR status was determined at the time of definitive surgery by a breast pathologist.

MRI Data Acquisition

MRI examinations were performed on a Philips 3T Achieva MR scanner (Philips Healthcare, Best, The Netherlands) and included both DCE-MRI and DW-MRI acquisitions. Prior to the DCE-MRI acquisition, data for constructing a T_1 map were acquired with an RF-spoiled 3D gradient echo multi-flip angle approach with ten flip angles from 2 to 20 degrees in 2° increments. For both the T_1 map and DCE scans, TR = 7.9 ms, TE = 4.6 ms, and the acquisition matrix was 192×192×20 (full-breast) over a sagittal square field of view (22 cm²) with slice thickness of 5 mm. The flip angle for DCE scans was 20 degrees. For the DCE study, each 20-slice set was collected in 16 seconds at 25 time points for just under seven minutes of dynamic scanning. A catheter placed within an antecubital vein delivered 0.1 mmol/kg (9 – 15 mL, depending on patient weight) of gadopentetate dimeglumine, Gd-DTPA, (Magnevist, Wayne, NJ) at 2 mL/sec (followed by a saline flush) *via* a power injector (Medrad, Warrendale, PA) after the acquisition of the first three dynamic scans (baseline).

DW-MRI was acquired with a single-shot spin echo (SE) echo planar imaging (EPI) sequence in three orthogonal diffusion encoding directions (x , y , and z). For 14 patients, $b = 0$ and 500 s/mm^2 , $TR/TE = 2500 \text{ ms}/45 \text{ ms}$, $\delta = 21.4 \text{ ms}$, $\delta = 10.3 \text{ ms}$ and 10 signal acquisitions were acquired. For 19 patients, $b = 0$ and 600 s/mm^2 , $TR/TE = \text{“shortest”}$ (range = $1800 - 3083 \text{ ms}/43 - 60 \text{ ms}$) = $20.7 - 29 \text{ ms}$, $\delta = 11.4 - 21 \text{ ms}$ and 10 signal acquisitions were acquired. For four patients, $b = 50$ and 600 s/mm^2 for two patients), $TR/TE = \text{“shortest”}$ (range = $1840 - 3593 \text{ ms}/43 - 60 \text{ ms}$) = $20.6 - 29 \text{ ms}$, $\delta = 11.5 - 21 \text{ ms}$ and 10 signal acquisitions were acquired. The acquisition matrix was $144 \times 144 \times 12$ over a (19.2 cm^2) field of view with a slice thickness of 5 mm and was obtained in 4 minutes and 40 seconds.

We note that subsets of this patient cohort have been included in a number of previous publications which focused on technical DCE-MRI or DW-MRI data acquisition methods ((16-22), and integrating such data into a predictive mathematical model of tumor growth ((23)).

Quantitative Image Analysis

For each patient at each time point, a region of interest (ROI) was manually drawn to completely surround the enhancing tumor as seen on each DCE-MRI tumor slice. The tumor was then defined as the voxels in each ROI displaying a signal intensity increase of greater than 80% after contrast injection. The threshold was calculated as

$\left(\frac{\bar{S}_{post} - \bar{S}_{pre}}{\bar{S}_{pre}} \right) \cdot 100$, where \bar{S}_{post} is the averaged post-contrast signal intensity and \bar{S}_{pre} is the average of the three pre-contrast time points. The threshold of 80% was selected as, in a previous study, it yielded the largest concordance correlation coefficient between the longest dimension of the tumor measured on the surgical specimen and the longest dimension measured on the DCE-MRI data just prior to surgery as reported previously (16). The DW-MRI data was rigidly registered (24) to the DCE-MRI data and the tumor ROIs as defined on the DCE-MRI data were then copied to the registered DW-MRI data so that tumor voxels on both data sets were co-aligned.

The Extended Tofts-Kety model (ETK) was used to estimate four physiological parameters from the DCE-MRI data: the volume transfer rate (K^{trans}), blood volume fraction (v_p), extravascular extracellular volume fraction (v_e), and the efflux rate constant ($k_{ep} = K^{trans}/v_e$). The arterial input function (AIF) was a population-averaged AIF constructed from 50 individual AIFs obtained through a semi-automatic AIF tracking algorithm (25). Voxels for which the ETK model did not converge, or converged to non-physical values (i.e., $K^{trans} > 5.0 \text{ min}^{-1}$, $v_e > 1.0$, $v_p > 1.0$, or any parameter below 0.0) were set equal to zero and not included in subsequent analyses.

ADC maps were calculated with the following equation: $ADC = \ln(S_1/S_2)/(b_2 - b_1)$, where S_1 and S_2 denote the signal acquired with b-values of b_1 and b_2 , respectively. Voxels for which the model could not fit the data or converged to non-physical values (i.e., $ADC > 3.0 \times 10^{-3} \text{ mm}^2/\text{s}$ or $ADC < 0.01 \times 10^{-3} \text{ mm}^2/\text{s}$) were set to zero and not included in subsequent analyses.

At the first two time points, longest dimension (LD), mean DCE-MRI parameters, and mean ADC values were computed for each patient and the changes of each parameter between t_1 and t_2 were calculated. The mean and change of the derived parameter k_{ep}/ADC were also obtained. The LD was measured from the tumor ROI estimated from the DCE-MRI data; for each slice with tumor voxels, the distance between any two voxels was calculated and the maximum distance in all slices was determined as the LD.

Statistical Analysis

All statistical analyses were performed using MATLAB R2012a (The Mathworks, Natick, MA). Receiver operator characteristic (ROC) curve analysis was performed to test the ability of each single parameter measurement as well as the derived parameter k_{ep}/ADC to predict pCR (26). “Optimal” cut-off points, sensitivities, specificities, and positive predictive values (PPV) were calculated to satisfy the Youden index; i.e., the point on the ROC curve that is furthest from chance and minimizes the overall rate of misclassification (27). The areas under the curve (AUC) were estimated using the trapezoidal rule. The non-parametric Wilcoxon rank sums test (28) was also used to detect if the parameters between the two response groups were significantly different.

To investigate if the AUC of k_{ep}/ADC was significantly different from the AUC of k_{ep} or ADC, the bootstrap method (29) was performed to generate the differences in AUC between k_{ep}/ADC and k_{ep} , and between k_{ep}/ADC and ADC with 1,000 replicates. The bootstrapped 95% confidence intervals (CI) for the AUC differences were then estimated.

RESULTS

Patient and Tumor Characteristics

Thirty-seven patients completed scanning at t_1 and 33 patients completed scanning at t_2 . The median age of the patients was 45 years old (range, 28 – 67 years). The median time between t_1 and t_2 was 14 days (range, 7 – 29 days). The median time between the first cycle of treatment administration and the post-1 cycle MRI was 1 day (range, 0 – 11 days). Table 1 summarizes the salient features of the study population, the receptor status, and the corresponding treatment regimens for all patients.

Pathological Response

At completion of neoadjuvant chemotherapy, 13 patients (35.1%) were defined as having achieved pCR. In the patients who did not achieve pCR, the median size of the residual tumor was 1.5 cm (range: 0.3 - 8 cm).

Representative Imaging Data

Figure 1 displays the K^{trans} , k_{ep} , v_e , v_p , and ADC maps, respectively, superimposed on anatomical T_1 -weighted images for a representative patient achieving pCR. The numbers under the panels indicate the mean values for each parameter at each time point. For this complete responder, both the mean K^{trans} and the mean k_{ep} decreased after one cycle of therapy (the changes are –11% and –26%, respectively), while the mean values of v_e , v_p , and ADC increased (16%, 2%, and 30%, respectively). Figure 2 displays similar data for a

non-pCR patient for which the mean K^{trans} , k_{ep} , and v_e increased by 22%, 15%, and 4%, respectively, after one cycle of treatment, while v_p and ADC decreased by 20% and 23%, respectively.

Predictive Performance of DCE- and DW-MR Data at t_1

Table 2 displays the ROC analysis of the pre-treatment data (i.e., LD, the DCE-MRI parameters, the ADC, and the parameter k_{ep}/ADC) to predict pathologic response. In this table, the cutoff point, sensitivity, specificity, PPV, and AUC, are listed for all the parameters. The table shows that the LD and DCE-MRI parameters (K^{trans} , k_{ep} , v_e , v_p , k_{ep}/ADC) all resulted in an AUC less than 0.7. The ADC data yielded a moderate AUC of 0.75, with sensitivity, specificity, and PPV of 1.00, 0.54, and 0.54, respectively, at the cutoff point of 1.2×10^{-3} mm²/s.

Predictive Performance of Changes in DCE- and DW-MRI from t_1 to t_2

33 patients were available for analyzing the changes of both the DCE-MRI and ADC data between the pre-therapy and post one cycle of therapy time points. The LD yielded an AUC of 0.68, with a sensitivity, specificity, and PPV of 0.92, 0.48, and 0.50, respectively. Among the four DCE-MRI parameters, the change of k_{ep} yielded the best AUC of 0.68, with a sensitivity, specificity, and PPV of 0.83, 0.63, and 0.59, respectively, at the cutoff point of -18.8%. The derived parameter k_{ep}/ADC yielded an AUC, sensitivity, specificity, and PPV of 0.72, 0.83, 0.63, and 0.59, respectively, at the cutoff point of -20.9%. These data are summarized in Table 3.

Predictive Performance of DCE- and DW-MRI at t_2

Both the DCE-MRI data and the ADC data after the first cycle of chemotherapy were available for 33 patients. Figure 3 displays the ROC curves and the optimal cut-off points for k_{ep} , ADC, and k_{ep}/ADC , respectively. The dotted line shows the ROC curve of k_{ep} alone, with the optimal cut-off point of 0.28 min^{-1} (marked as a triangle) and the dashed line shows the ROC curve for ADC alone, with the optimal point of $1.4 \text{ mm}^2/\text{s} \times 10^{-3}$ (marked as a star). The solid line displays the ROC curve for k_{ep}/ADC , with the optimal point of 3.32 1/mm^2 (marked as a star). k_{ep} yielded an AUC, sensitivity, specificity, and PPV of 0.77, 0.83, 0.65, and 0.59, respectively. ADC yielded an AUC, sensitivity, specificity, and PPV of 0.81, 0.83, 0.67, and 0.59, respectively. The derived parameter k_{ep}/ADC achieved an AUC, sensitivity, specificity, and PPV of 0.86, 0.92, 0.75, and 0.69, respectively. The LD yielded an AUC of only 0.58, with the sensitivity, specificity, and PPV of 0.92, 0.38, and 0.46, respectively. These data are summarized in Table 4.

Figure 4 shows boxplots of k_{ep} , ADC, and k_{ep}/ADC for pCRs and non-pCRs. The lines within the boxes denote the median and the bottom and top edges of the boxes denote the 25th and 75th percentiles, respectively. The medians of k_{ep} for non-pCRs and pCRs were 0.32 min^{-1} and 0.23 min^{-1} ($P = 0.013$), respectively, while they were $1.24 \text{ mm}^2/\text{s} \times 10^{-3}$ and $1.59 \text{ mm}^2/\text{s} \times 10^{-3}$ for ADC ($P = 0.0037$), and 4.27 1/mm^2 and 2.63 1/mm^2 for k_{ep}/ADC ($P = 0.00087$), respectively.

Figure 5 shows the distributions of the AUC differences between k_{ep}/ADC and k_{ep} , and between k_{ep}/ADC and ADC generated by the bootstrap method. The bootstrapped 95% CIs of the AUC differences between k_{ep}/ADC and k_{ep} were (0.0062, 0.20), indicating that the AUCs between k_{ep}/ADC and k_{ep} were significantly different. Although the 95% bootstrap CIs of the AUC differences between k_{ep}/ADC and ADC included zero (-0.12, 0.24), the figure clearly shows a trend approaching significance.

DISCUSSION

To our knowledge, this is the first report of a derived multiparametric quantitative MRI measurement predicting pCR following breast cancer NAC. We chose to study the derived parameter k_{ep}/ADC for statistical and physiological reasons. The hypothesis is that in the case of positive response k_{ep} would decrease and ADC would increase, whereas in the case of negative response (i.e., progressive disease) k_{ep} would increase and ADC would decrease. Thus, the ratio k_{ep}/ADC has the potential to increase the statistical separation between patients going on to achieve pCR versus those who do not (see Figure 4). For this practical reason, the ratio k_{ep}/ADC is a reasonable parameter to consider; indeed, such derived parameters have been utilized before, even in the particular case of assessing therapeutic response of breast cancer in the neoadjuvant setting (see, e.g., 30).

Our results show that the combined parameter k_{ep}/ADC was able to predict pCR with greater accuracy (AUC = 0.86) than either k_{ep} (AUC = 0.77) or ADC (AUC = 0.81) in isolation. The bootstrap method showed that the AUCs between k_{ep}/ADC and k_{ep} were significantly different and the AUCs between k_{ep}/ADC and ADC showed a trend approaching significance. Although these results may be considered preliminary due to our small sample size, we consider them encouraging signs of the potentials of multiparametric MR imaging to depict tumor biology and assess tumor response to therapy early in the course of treatment (31). Thus, we believe this study contributes to the growing body of knowledge in this developing area.

A secondary finding in this study is that data obtained after the first cycle of therapy was the most statistically robust for predicting eventual treatment response. Many previous studies have focused on either pre-treatment data or the change between pre-treatment data and data acquired after one or two cycles of chemotherapy (6-8). Only the study by Fangberget *et al* (14) reported that the mean ADC values after four cycles of NAC showed a significant difference between the patients in the pCR and non-pCR groups, while the percent change of ADC did not. In our study, we found that the mean parameters of both the DCE- and DW-MRI data after one cycle of therapy yielded a better performance (as measured by ROC analysis) than either the pre-treatment data or the percent change of the parameters.

There are a number of limitations of this study. First, the temporal resolution of 16 s is not optimal for characterizing the arterial input function and this can confound a quantitative DCE-MRI analysis. This temporal resolution was chosen as a compromise between temporal and spatial resolution and field of view coverage (please refer to (16) for an in-depth discussion). Second, a population AIF was used to estimate the DCE-MRI parameters. In practice, it is difficult to estimate reliable AIFs at each scanning session for each patient.

Hence, we used a population AIF as an alternative approach. Third, the treatment regimens used in this study were left to the discretion of the treating physicians, and were therefore quite varied. It is certainly possible that the imaging biomarkers could vary by both the biology of the disease as well as by the agents utilized. When this is combined with the modest sample size (data was available on 37 patients before NAC, while we were able to acquire data on 33 patients both before and after one cycle of NAC), our findings are preliminary in nature and will need to be validated in larger prospective trials.

In summary, our study shows that combining DCE- and DW-MRI data into a single derived multiparametric measurement k_{ep}/ADC can increase the ability to predict breast cancer response to NAC at a very early time point. It may allow clinicians to tailor therapy on an individual basis. Future work includes investigating multivariate analysis of DCE- and DW-MRI on a larger cohort of patients.

Acknowledgments

Grant Support: NCI 1U01CA142565, NCI 1U01CA174706, NCI 1P50 098131, NCI P30 CA068485, NCRR/NIH UL1 RR024975-01 (Vanderbilt CTSA grant)

References

1. Yankeelov TE, Arlinghaus LR, Li X, Gore JC. The role of magnetic resonance imaging biomarkers in clinical trials of treatment response in cancer. *Semin Oncol.* 2011; 38:16–25. [PubMed: 21362513]
2. Guo Y, Cai YQ, Cai ZL, Gao YG, An NY, Ma L, Mahankali S, Gao JH. Differentiation of clinically benign and malignant breast lesions using diffusion-weighted imaging. *J Magn Reson Imaging.* 2002; 16:172–178. [PubMed: 12203765]
3. Cheung YC, Chen SC, Su MY, See LC, Hsueh S, Chang HK, Lin YC, Tsai CS. Monitoring the size and response of locally advanced breast cancers to neoadjuvant chemotherapy (weekly paclitaxel and epirubicin) with serial enhanced MRI. *Breast Cancer Res Treat.* 2003; 78:51–58. [PubMed: 12611457]
4. Chou CP, Wu MT, Chang HT, Lo YS, Pan HB, Degani H, Furman-Haran E. Monitoring breast cancer response to neoadjuvant systemic chemotherapy using parametric contrast-enhanced MRI: a pilot study. *Acad Radiol.* 2007; 14:561–573. [PubMed: 17434070]
5. Martincich L, Montemurro F, De Rosa G, Marra V, Ponzzone R, Cirillo S, Gatti M, Biglia N, Sarotto I, Sismondi P, Regge D, Aglietta M. Monitoring response to primary chemotherapy in breast cancer using dynamic contrast-enhanced magnetic resonance imaging. *Breast Cancer Res Treat.* 2004; 83:67–76. [PubMed: 14997056]
6. Yankeelov TE, Lepage M, Chakravarthy A, Broome EE, Niermann KJ, Kelley MC, Meszoely I, Mayer IA, Herman CR, McManus K, Price RR, Gore JC. Integration of quantitative DCE-MRI and ADC mapping to monitor treatment response in human breast cancer: initial results. *Magn Reson Imaging.* 2007; 25:1–13. [PubMed: 17222711]
7. Ah-See ML, Makris A, Taylor NJ, Harrison M, Richman PI, Burcombe RJ, Stirling JJ, d'Arcy JA, Collins DJ, Pittam MR, Ravichandran D, Padhani AR. Early changes in functional dynamic magnetic resonance imaging predict for pathologic response to neoadjuvant chemotherapy in primary breast cancer. *Clin Cancer Res.* 2008; 14:6580–6589. [PubMed: 18927299]
8. Padhani AR, Hayes C, Assersohn L, Powles T, Makris A, Suckling J, Leach MO, Husband JE. Prediction of clinicopathologic response of breast cancer to primary chemotherapy at contrast-enhanced MR imaging: initial clinical results. *Radiology.* 2006; 239:361–374. [PubMed: 16543585]
9. Pickles MD, Gibbs P, Lowry M, Turnbull LW. Diffusion changes precede size reduction in neoadjuvant treatment of breast cancer. *Magn Reson Imaging.* 2006; 24:843–847. [PubMed: 16916701]

10. Sharma U, Danishad KK, Seenu V, Jagannathan NR. Longitudinal study of the assessment by MRI and diffusion-weighted imaging of tumor response in patients with locally advanced breast cancer undergoing neoadjuvant chemotherapy. *NMR Biomed.* 2009; 22:104–113. [PubMed: 18384182]
11. Belli P, Costantini M, Ierardi C, Bufi E, Amato D, Mule A, Nardone L, Terribile D, Bonomo L. Diffusion-weighted imaging in evaluating the response to neoadjuvant breast cancer treatment. *Breast J.* 2011; 17:610–619. [PubMed: 21929557]
12. Woodhams R, Kakita S, Hata H, Iwabuchi K, Kuranami M, Gautam S, Hatabu H, Kan S, Mountford C. Identification of residual breast carcinoma following neoadjuvant chemotherapy: diffusion-weighted imaging--comparison with contrast-enhanced MR imaging and pathologic findings. *Radiology.* 2010; 254:357–366. [PubMed: 20093508]
13. Nilsen L, Fangberget A, Geier O, Olsen DR, Seierstad T. Diffusion-weighted magnetic resonance imaging for pretreatment prediction and monitoring of treatment response of patients with locally advanced breast cancer undergoing neoadjuvant chemotherapy. *Acta Oncol.* 2010; 49:354–360. [PubMed: 20397769]
14. Fangberget A, Nilsen LB, Hole KH, Holmen MM, Engebraaten O, Naume B, Smith HJ, Olsen DR, Seierstad T. Neoadjuvant chemotherapy in breast cancer--response evaluation and prediction of response to treatment using dynamic contrast-enhanced and diffusion-weighted MR imaging. *Eur Radiol.* 2011; 21:1188–1199. [PubMed: 21127880]
15. Wu LM, Hu JN, Gu HY, Hua J, Chen J, Xu JR. Can diffusion-weighted MR imaging and contrast-enhanced MR imaging precisely evaluate and predict pathological response to neoadjuvant chemotherapy in patients with breast cancer? *Breast Cancer Res Treat.* 2012; 135:17–28. [PubMed: 22476850]
16. Blinded1
17. Blinded2
18. Blinded3
19. Blinded4
20. Blinded5
21. Blinded6
22. Blinded7
23. Blinded8
24. Maes F, Collignon A, Vandermeulen D, Marchal G, Suetens P. Multimodality image registration by maximization of mutual information. *IEEE Trans Med Imaging.* 1997; 16:187–198. [PubMed: 9101328]
25. Li X, Welch EB, Chakravarthy AB, Lei X, Arlinghaus LR, Farley J, Loveless ME, Mayer I, Kelley M, Meszoely I, Means-Powell J, Abramson V, Grau A, Gore JC, Yankeelov TE. A Novel AIF Detection Method and a Comparison of DCE-MRI Parameters Using Individual and Population Based AIFs in Human Breast Cancer. *Phys Med Biol.* 2011; 56:5753–5769. [PubMed: 21841212]
26. Hanley JA, McNeil BJ. The meaning and use of the area under a receiver operating characteristic (ROC) curve. *Radiology.* 1982; 143:29–36. [PubMed: 7063747]
27. Perkins NJ, Schisterman EF. The inconsistency of "optimal" cutpoints obtained using two criteria based on the receiver operating characteristic curve. *Am J Epidemiol.* 2006; 163:670–675. [PubMed: 16410346]
28. Lehmann EL. Parametric versus nonparametrics: two alternative methodologies. *Journal of Nonparametric Statistics.* 2009; 21:397–405.
29. Efron, B.; Tibshirani, RJ. *An Introduction of the Bootstrap.* Chapman and Hall/CRC; New York: 1993.
30. Cerussi AE, Tanamai VW, Hsiang D, Butler J, Mehta RS, Tromberg BJ. Diffuse optical spectroscopic imaging correlates with final pathological response in breast cancer neoadjuvant chemotherapy. *Phil. Trans. R. Soc. A.* 2011; 369:4512–4530. [PubMed: 22006904]
31. Padhani AR, Miles KA. Multiparametric imaging of tumor response to therapy. *Radiology.* 2010; 256:348–364. [PubMed: 20656830]

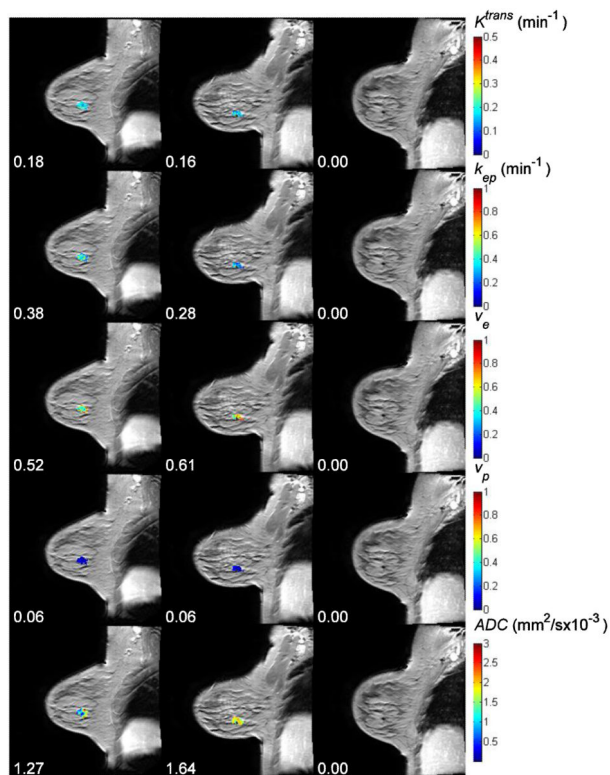


Figure 1.

The averaged post-contrast MR images with K^{trans} , k_{ep} , v_e , v_p , and ADC maps superimposed at three time points (three columns) for one pathological complete responder. The numbers under panels are the mean values for K^{trans} , k_{ep} , v_e , v_p , and ADC at different time points. For this complete responder, both the mean K^{trans} and the mean k_{ep} were decreased after one cycle of therapy, while the mean values of v_e , v_p , and ADC were increased.

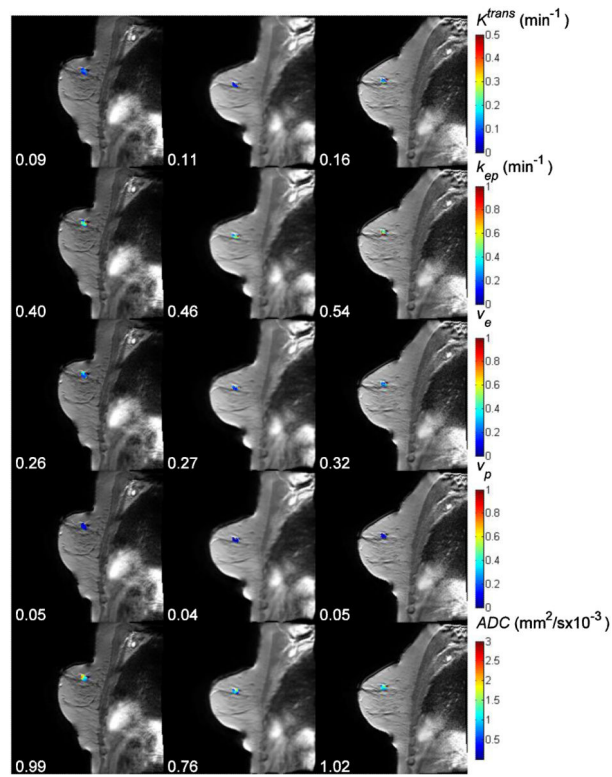


Figure 2. The averaged post-contrast MR images with K^{trans} , k_{ep} , v_e , v_p , and ADC maps superimposed at three time points (three columns) for one non-pCR. The numbers under panels are the mean values for K^{trans} , k_{ep} , v_e , v_p , and ADC at different time points.

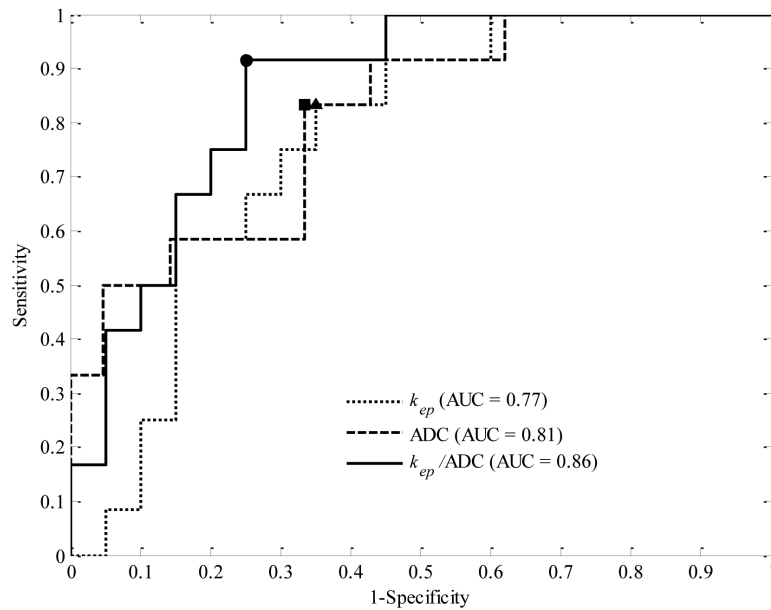


Figure 3.

ROC for k_{ep} (dotted line), ADC (dashed line), and k_{ep}/ADC (solid line). k_{ep} and ADC alone yielded an AUC of 0.77 and 0.81 with the optimal cut-off point of 0.28 min^{-1} and $1.4 \text{ mm}^2/\text{s} \times 10^{-3}$ (marked as a triangle and a square), respectively, while k_{ep}/ADC had an AUC of 0.86 with the optimal cut-off point of 3.32 1/mm^2 (marked as a dot). The sensitivity, specificity, and PPV at the cut-off points are 0.83, 0.65, and 0.59 for k_{ep} , 0.83, 0.67, and 0.59 for ADC, and 0.92, 0.75, and 0.69 for k_{ep}/ADC , respectively.

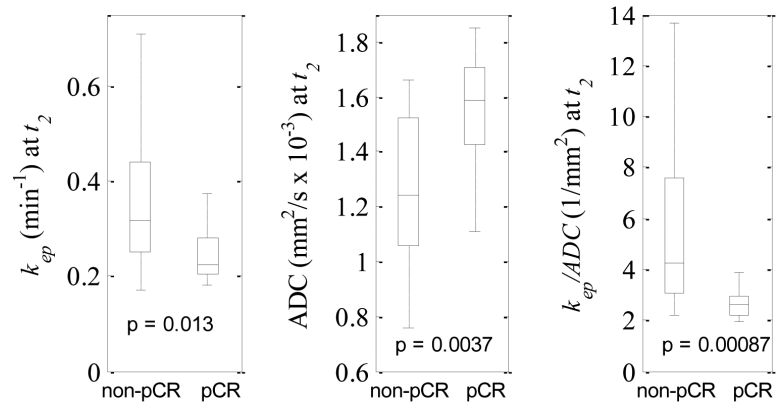


Figure 4.

Boxplots of k_{ep} (left panel), ADC (middle panel), and k_{ep}/ADC (right panel) at t_2 for non-pCRs and pCRs. The central marks show the median and the edges of the box are the 25th and 75th percentiles. Outliers are not shown in the figure. The medians of k_{ep} for non-pCRs and pCRs were 0.32 min^{-1} and 0.23 min^{-1} , respectively, while they were $1.24 \text{ mm}^2/\text{s} \times 10^{-3}$ and $1.59 \text{ mm}^2/\text{s} \times 10^{-3}$ for ADC, and $4.27 \text{ 1}/\text{mm}^2$ and $2.63 \text{ 1}/\text{mm}^2$ for k_{ep}/ADC , respectively.

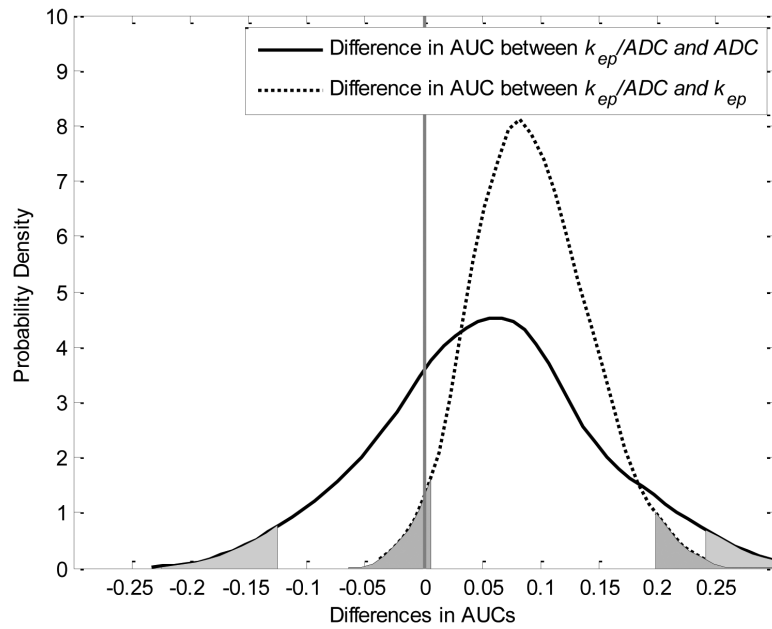


Figure 5.

The figure displays density distributions of the AUC differences between k_{ep}/ADC and k_{ep} (dotted line), and between k_{ep}/ADC and ADC (solid line) after one cycle of NAC. The 95% CIs of the AUC differences between k_{ep}/ADC and k_{ep} were (0.0062, 0.20), while the 95% CIs of the AUC differences between k_{ep}/ADC and ADC were (-0.12, 0.24). The areas outside the 95% CIs are shaded for both distributions.

Table 1

Clinical features of the study population.

Patient #	Age (yr)	Treatment Regimens	Receptor status			Tumor grade	Excised tumor size	Pathologic response	Surgery
			ER	PR	HER2				
1	50	dd AC × 4 → Taxol × 12	+	+	-	3	0.5	Residual disease	mastectomy
2	52	dd Taxotere × 4	+	-	+	3	1.5	Residual disease	mastectomy
3	60	dd AC × 2 → Taxol-Herceptin × 12	+	+	+	1	2.9	Residual disease	mastectomy
4	36	cisplatin/taxol +/- RAD001 × 12	-	-	-	2	2.9	Residual disease	mastectomy
5	48	dd AC × 4 → Taxol × 4	+	+	-	1	1.3	Residual disease	mastectomy
6	43	dd AC × 4 → Taxol × 4	+	+	-	2	2.6	Residual disease	mastectomy
7	59	dd AC × 4 → Taxol × 4	+	+	-	2	4.2	Residual disease	mastectomy
8	53	cisplatin/taxol +/- RAD001 × 12	-	-	-	2	1.3	Residual disease	mastectomy
9	35	Trastuzumab + Carboplatin + Ixabepilone × 6	+	+	+	3	1.4	Residual disease	mastectomy
10	28	cisplatin/taxol +/- RAD001 × 12	-	-	-	3	0.8	Residual disease	mastectomy
11	33	AC × 4 → Taxol × 12	+	+	-	3	1.2	Residual disease	mastectomy
12	39	AC × 4 → Taxol × 12	+	+	-	1	2.5	Residual disease	mastectomy
13	57	AC × 4 → Taxol × 12	-	-	-	3	N/A	Residual disease	progressed with brain mets
14	67	AC × 4 → Taxol/Herceptin × 12	-	-	+	3	1.8	Residual disease	mastectomy
15	45	cisplatin/taxol +/- RAD001 × 12	-	-	-	3	0.5	Residual disease	mastectomy
16	46	Taxotere/Carboplatin/Herceptin × 6	+	+	+	3	0.3	Residual disease	mastectomy
17	47	Taxotere × 3 → dd AC × 4	+	+	-	1	8.0	Residual disease	mastectomy
18	36	ddAC × 4 → Taxol × 12	+	+	+	2	1.0	Residual disease	mastectomy
19	43	cisplatin/taxol +/- RAD001 × 12	-	-	+	3	0.7	Residual disease	mastectomy
20	55	ddAC × 4 → Taxol × 10	+	+	-	2	3.5	Residual disease	mastectomy
21	58	cisplatin/taxol +/- RAD001 × 12	-	+	-	2	1.7	Residual disease	mastectomy
22	36	ddAC × 4 → Taxol × 12	+	+	-	2	2.1	Residual disease	mastectomy
23	43	cisplatin/taxol +/- RAD001 × 12	-	-	-	3	1.4	Residual disease	mastectomy
24	42	cisplatin/taxol +/- RAD001 × 6	+	+	-	2	3.5	Residual disease	mastectomy
25	53	dd AC × 4 → Taxol-Herceptin × 7	-	-	+	3	0	pCR	mastectomy
26	46	ddTaxotere → AC	-	+	-	3	0	pCR	mastectomy
27	46	dd AC × 4 → Taxol-Herceptin × 12	-	-	+	2	0	pCR	mastectomy
28	33	ddAC × 4 → Taxol × 12	-	-	-	3	0	pCR	mastectomy
29	39	Trastuzumab and Lapatinib × 12	-	-	+	2	0	pCR	mastectomy
30	46	ddAC × 4 → Taxol × 12	+	-	-	3	0	pCR	mastectomy
31	42	cisplatin/taxol +/- RAD001 × 12	-	-	-	3	0	pCR	mastectomy
32	34	ddTaxotere → AC	-	-	-	3	0	pCR	mastectomy
33	44	Trastuzumab and Lapatinib × 12	-	-	+	3	0	pCR	mastectomy
34	37	cisplatin/taxol +/- RAD001 × 11	-	-	-	3	0	pCR	mastectomy
35	39	ddAC × 4 → Taxol × 10	-	-	-	3	0	pCR	mastectomy
36	48	Taxotere/Carboplatin/Herceptin × 5	-	-	+	3	0	pCR	mastectomy
37	51	ddAC × 4 → Taxol × 12	-	-	-	3	0	pCR	mastectomy

§The study is ongoing and we are blinded to the randomization.

This patient was transferred to another hospital and the tumor size is not available.

Author Manuscript

Author Manuscript

Author Manuscript

Author Manuscript

Table 2ROC analysis of the parameters at t_I .

Parameter	Cutoff	Sensitivity	Specificity	PPV	AUC
LD	1.92 (cm)	1.00	0.33	0.45	0.66
ADC	$1.2 (\times 10^{-3} \text{ mm}^2/\text{s})$	1.00	0.54	0.54	0.75
K^{trans}	0.15 (min^{-1})	0.77	0.50	0.48	0.59
k_{ep}	0.45 (min^{-1})	0.85	0.32	0.42	0.49
v_e	0.41	0.62	0.55	0.44	0.52
v_p	0.07	0.92	0.32	0.44	0.55
k_{ep}/ADC	5.18 ($1/\text{mm}^2$)	0.77	0.55	0.50	0.59

Author Manuscript

Author Manuscript

Author Manuscript

Author Manuscript

Table 3ROC analysis of parameter changes from t_1 to t_2 .

Parameter	Cutoff	Sensitivity	Specificity	PPV	AUC
LD	-1.0%	0.92	0.48	0.50	0.68
ADC	5.5%	0.50	0.76	0.55	0.62
K^{trans}	12.7%	1.00	0.37	0.50	0.57
k_{ep}	-18.8%	0.83	0.63	0.59	0.68
v_e	92.4%	1.00	0.11	0.41	0.41
v_p	75.0%	1.00	0.26	0.46	0.55
k_{ep}/ADC	-20.9%	0.83	0.63	0.59	0.72

Author Manuscript

Author Manuscript

Author Manuscript

Author Manuscript

Table 4ROC analysis of the parameters at t_2 .

Parameter	Cutoff	Sensitivity	Specificity	PPV	AUC
LD	1.91 (cm)	0.92	0.38	0.46	0.58
ADC	$1.4 (\times 10^{-3} \text{ mm}^2/\text{s})$	0.83	0.67	0.59	0.81
K^{trans}	0.1 (min^{-1})	0.67	0.75	0.62	0.68
k_{ep}	0.28 (min^{-1})	0.83	0.65	0.59	0.77
v_e	0.65	0.17	0.95	0.67	0.52
v_p	0.04	0.50	0.80	0.60	0.62
k_{ep}/ADC	3.32 ($1/\text{mm}^2$)	0.92	0.75	0.69	0.86

Author Manuscript

Author Manuscript

Author Manuscript

Author Manuscript